Key driving forces in the biosynthesis of autoinducing peptides required for staphylococcal virulence

Boyuan Wang[a,b], Aishan Zhao[a], Richard P. Novick[c], and Tom W. Muir[a,1]

[a]Department of Chemistry, Frick Chemistry Laboratory, Princeton University, Princeton, NJ 08544; [b]Graduate Program, The Rockefeller University, New York, NY 10065; and [c]Department of Microbiology, Skirball Institute, New York University Medical Center, New York, NY 10016

Edited by James A. Wells, University of California, San Francisco, CA, and approved July 17, 2015 (received for review March 26, 2015)

Staphylococci produce autoinducing peptides (AIPs) as quorum-sensing signals that regulate virulence. These AIPs feature a thiolactone macrocycle that connects the peptide C terminus to the side chain of an internal cysteine. AIPs are processed from ribosomally synthesized precursors [accessory gene regulator D (AgrD)] through two proteolytic events. Formation of the thiolactone is coupled to the first of these and involves the activity of the integral membrane protease AgrB. This step is expected to be thermodynamically unfavorable, and therefore, it is unclear how AIP-producing bacteria produce sufficient amounts of the thiolactone-containing intermediate to drive quorum sensing. Herein, we present the in vitro reconstitution of the AgrB-dependent proteolysis of an AgrD precursor from *Staphylococcus aureus*. Our data show that efficient thiolactone production is driven by two unanticipated features of the system: (*i*) membrane association of the thiolactone-containing intermediate, which stabilizes the macrocycle, and (*ii*) rapid degradation of the C-terminal proteolysis fragment $AgrD^C$, which affects the reaction equilibrium position. Cell-based studies confirm the intimate link between AIP production and intracellular $AgrD^C$ levels. Thus, our studies explain the chemical principles that drive AIP production, including uncovering a hitherto unknown link between quorum sensing and peptide turnover.

Staphylococcus aureus | quorum sensing | thiolactone | protein homeostasis | thermodynamics of proteolysis

Quorum sensing (QS) is a process in which individual microbes produce and sense a diffusive signaling molecule (known as the autoinducer) to coordinate behaviors of the population (1). In the commensal pathogen *Staphylococcus aureus*, QS is required for the synchronized adjustment of gene expression patterns that ultimately enables the pathogen to establish an infection and endure the immune defense of the mammalian host (2, 3). The chromosomal locus that encodes this QS machinery is called the accessory gene regulator (*agr*). The autoinducer, autoinducing peptide (AIP), contains a thiolactone ring formed by condensation of the C-terminal carboxyl group and the sulfhydryl group of an internal cysteine (Fig. 1*A*, *Inset*). The resulting macrocycle is absolutely necessary for binding of the peptide to its receptor AgrC (2) and conserved in the autoinducer peptides produced by a plethora of low-GC, Gram-positive pathogens, with variations to oxolactones seen in a few cases (4, 5).

AIP biosynthesis is of particular interest to us, because formation of the high-energy thiolactone linkage is thought to not be coupled to ATP hydrolysis. It is unclear how the bacteria overcome the thermodynamic challenge to produce AIP at a rate sufficient for punctual QS induction. In the current AIP biosynthesis model (Fig. 1*A*, black arrows), the peptide is ribosomally translated as a precursor, AgrD, in which the mature AIP sequence is flanked by an N-terminal leader peptide and a C-terminal recognition sequence (6). The N-terminal leader forms an amphipathic helix, which attaches the precursor to the inner leaflet of the cell membrane (7). In the first step, AgrD is processed by a membrane-integrated peptidase, AgrB, such that the C-terminal recognition sequence ($AgrD^C$) is removed with concomitant installation of the thiolactone (Fig. 1*A*, step 1) (8, 9). This intermediate, herein referred to as AgrD(1–32)-thiolactone, is then translocated to the extracellular leaflet of the cell membrane, where the general signal peptidase SpsB is thought to clip off the N-terminal leader peptide (10), releasing AIP to the extracellular space (Fig. 1*A*, step 2). The first proteolytic event in this process is reminiscent of the ring closure step in the biosynthesis of a spectrum of lactam-containing ribosomal peptide natural products, including cyanobactins, amatoxins, cyclotides, and orbitides (11). However, although lactam formation through peptidyl transfer is roughly isoenthalpic (and hence, entropically driven overall), thiolactone formation through an analogous process is expected to be an enthalpically uphill process and thus, overall thermodynamically less favorable. We note that, although the pathway discussed above is generally accepted, the existence of the thiolactone intermediate has not been unambiguously proven (9, 12). Thus, an alternative and thermodynamically reasonable pathway could involve a process in which AgrD is first cleaved by AgrB to give a linear AgrD(1–32) peptide, which is then cyclized to give the AgrD(1–32)-thiolactone on, for example, ATP-dependent activation on the C-terminal carboxylate (Fig. 1*A*, dashed arrows). A full understanding of thiolactone formation in the AIP, therefore, necessitates precise characterization of the product of step 1 and if cyclization occurs, demonstration of its spontaneity under physiologically relevant conditions.

Herein, we present the in vitro reconstitution of the first step in AIP biosynthesis using highly purified recombinant or synthetic reagents. AgrB from *S. aureus* forms stable dimers and is functional only when embedded in lipid bilayers. AgrB catalyzes the efficient, reversible cyclization of AgrD into the thiolactone intermediate alongside a slow, irreversible hydrolysis reaction that gives the linear AgrD(1–32) fragment. From a quasiequilibrium

Significance

Autoinducing peptide (AIP), a cyclic peptide produced by the bacterium *Staphylococcus aureus* for intercellular communication, contains a high-energy thiolactone linkage. This linkage is proposed to form directly from the proteolysis of a stable peptide bond without free energy input from ATP hydrolysis. Using highly purified protein/peptide components, we reconstitute this proteolysis event and show that this reaction is powered collectively by the stabilization of the thiolactone product as a consequence of membrane partitioning and the degradation of the concomitantly released C-terminal fragment. Rapid turnover of the C fragment is required for efficient AIP production in vivo, indicating a connection between protein homeostasis and intercellular signaling in *S. aureus*.

Author contributions: B.W. and T.W.M. designed research; B.W. and A.Z. performed research; B.W. and A.Z. contributed new reagents/analytic tools; B.W., A.Z., R.P.N., and T.W.M. analyzed data; and B.W. and T.W.M. wrote the paper.

The authors declare no conflict of interest.

This article is a PNAS Direct Submission.

[1]To whom correspondence should be addressed. Email: muir@princeton.edu.

This article contains supporting information online at www.pnas.org/lookup/suppl/doi:10.1073/pnas.1506030112/-/DCSupplemental.

BIOCHEMISTRY

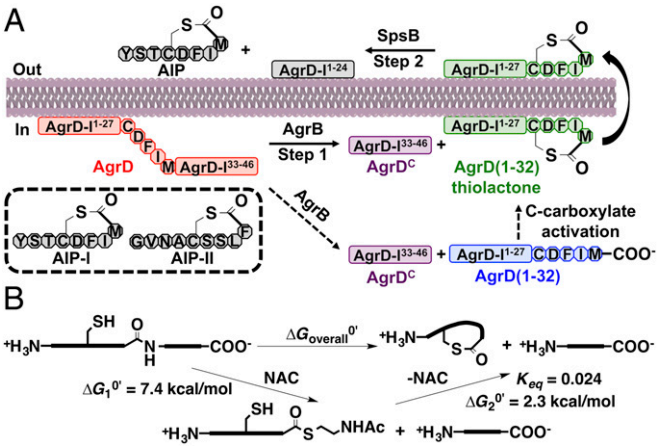

Fig. 1. AIP biosynthesis and models for free energy change estimation for the thiolactone formation. (*A*) Models of AIP production in *S. aureus* cells as exemplified by processing of AgrD-I. The generally accepted pathway and an alternative pathway are depicted using black and dashed arrows, respectively. (*Inset*) Sequences of AIPs produced by *agr* variants I and II. (*B*) A two-step model that recapitulates the thiolactone formation from a linear peptide. Estimated values of free energy change and/or equilibrium constant are shown for each step. Details are in the text.

state involving AgrD, AgrD(1–32)-thiolactone, and the AgrD^C fragment, we determined the equilibrium constant of the cyclization. Our data suggest that the bacterium can maintain a reasonable intracellular level of thiolactone intermediate only when the turnover of AgrD^C through additional proteolysis is efficient. Membrane targeting of this intermediate by the N-terminal leader sequence induces lipid partitioning of the macrocycle and thereby, enhances its stability against ring-opening thiolysis. This effect partly ameliorates the enthalpic deficit of the thiolactone formation and renders the reaction more permissible than would otherwise be expected.

Results

Estimation of the Free Energy Cost Associated with Thiolactone Formation. To get a better picture of the thermodynamic challenge associated with conversion of AgrD into a thiolactone, we first estimated the ΔG for the reaction based on existing data on analogous model reactions. A two-step process would recapitulate such a reaction: the scissile peptide bond first undergoes thiolysis with a CoA mimic, *N*-acetylcysteamine (NAC), to give an N-terminal thioester fragment and an unmodified C fragment (Fig. 1*B*), and the N-terminal fragment subsequently cyclizes into a thiolactone to release NAC (Fig. 1*B*). The standard ΔG conditioned at pH 7 of step 1, $\Delta G_1^{0,} = 7.4$ kcal/mol, is assigned according to the well-documented data for the hydrolysis of a Gly-Gly peptide bond or a thioester bond in acetyl-CoA (details in *SI Appendix*) (13, 14). With respect to step 2, we assume that the macrocycle resembles an unstrained large ring and that the ring closure is isoenthalpic. As a consequence, the equilibrium constant (K_{eq}) of this ring closure should stay between 0.01 and 0.05 M as predicted from the effective molarity for the cyclization of a bifunctional molecule into a large ring (details in *SI Appendix*) (15). This interval corresponds to a $\Delta G_2^{0,}$ value ranging from 1.8 to 2.8 kcal/mol. We, hence, used $\Delta G_2^{0,} = 2.3$ kcal/mol to calculate the $\Delta G^{0,}_{overall}$ and the $K_{eq,\ overall}$ for the strain-free thiolactone formation from a generic peptide (Eqs. **1** and **2**):

$$\Delta G^{0,}_{\text{overall}} = \Delta G^{0,}_1 + \Delta G^{0,}_2 = 9.7 \text{ kcal/mol} \qquad [1]$$

and

$$K_{\text{eq, overall}} = \exp\left(-\Delta G^{0,}_{\text{overall}}/RT\right) = 1.4 \times 10^{-7}. \qquad [2]$$

The estimated $K_{eq,\ overall}$, if applied to the AgrD(1–32)-thiolactone formation from AgrD, would restrict the intracellular abundance of the former to a level incompatible with the AIP production rate required for *agr* autoinduction (*Discussion*). Therefore, assuming the thiolactone intermediate to be the direct product of AgrB-mediated proteolysis in vivo, some mechanism must exist to render the reaction more permissible.

Expression and Purification of Recombinant AgrB and AgrD Constructs. Four *agr* allelic variants have been found in *S. aureus*, each producing an AIP with distinctive QS specificity (6, 16). We elected to study the AgrB and AgrD from alleles *agr-I* and *agr-II* in our reconstitution studies. The current model of AIP biosynthesis has been developed primarily based on cells possessing an *agr-I* allele, which is significantly diverged from *agr-II*: AgrB-II and AgrD-II share 61% and 48% sequence identity with AgrB-I and AgrD-I, respectively. Importantly, genetic studies show that heterologous processing of AgrD is forbidden between these two alleles (6).

WT AgrD-I and AgrD-II as well as N-terminally FlagHis$_6$-tagged versions thereof were generated using a recombinant fusion protein strategy (*SI Appendix*, Figs. S1 *A* and *B* and S9 and Table S1). AgrB-I and AgrB-II were overexpressed in *Escherichia coli* as His$_6$-tagged recombinant proteins and purified (*SI Appendix*, Fig. S1*C*). Surprisingly, AgrB-I and AgrB-II showed multiple bands when analyzed by SDS/PAGE, despite being chemically homogeneous as indicated by MS (*SI Appendix*, Fig. S1*D*). Suspecting that this behavior reflected oligomerization of the protein, we used chemical cross-linking as well as a nanodisc reconstitution assay (17) to show that AgrB forms proteolytically active, stable dimers in lipid layers (*SI Appendix*, Fig. S2).

AgrD(1–32)-Thiolactone Is the Major Product of the AgrB-Catalyzed Proteolysis of AgrD. We next set out to characterize the products of AgrB-mediated proteolysis of AgrD. To this end, AgrB and AgrD (from *agr-I* or *agr-II*) were coreconstituted into liposomes composed of 1-palmitoyl-2-oleyl-phosphatidylcholine (POPC) and 1-palmitoyl-2-oleyl-phosphatidylglyerol (POPG) at a ratio of 3:1. This lipid composition was selected based on preliminary proteolysis assays using AgrB embedded in liposomes comprised of POPC-POPG mixtures at different ratios (*SI Appendix*, Fig. S3 *A* and *B*) (18). Tris-Tricine SDS/PAGE revealed efficient proteolysis occurring between cognate AgrB–AgrD pairs but not heterologous ones (*SI Appendix*, Fig. S3*C*). Additional characterization of the proteolysis products of nontagged AgrD-I and AgrD-II was achieved using reverse-phase (RP) -HPLC and MS (Fig. 2*A*). For each reaction, RP-HPLC/MS identified three products in addition to the starting material, namely AgrD^C, AgrD(1–32)-thiolactone, and linear AgrD(1–32) (Fig. 2 *B*–*E*). Importantly, the thiolactone is the major AgrD(1–32) fragment in both reactions (Fig. 2 *B*, green arrow and *D*, green arrow), which is in line with the AIP biosynthesis model depicted by black arrows in Fig. 1*A*. We, therefore, refer to the AgrB-catalyzed processing of AgrD as the "proteolytic cyclization."

AgrD Processing by AgrB Is a Reversible Process. In our initial reconstitution trials, complete consumption of AgrD was never observed, despite significant production of AgrD(1–32)-thiolactone. To account for this finding, we speculated that the proteolytic cyclization might have reached a balanced equilibrium under our reaction conditions. To test this idea, we treated AgrD-I (the FlagHis$_6$-tagged version; 20 μM) with proteoliposomes containing 1 μM AgrB-I and analyzed the reaction mixture by RP-HPLC at a series of time points (Fig. 3*A*). We observed time-dependent consumption of the starting material as well as the production of three additional species identified by

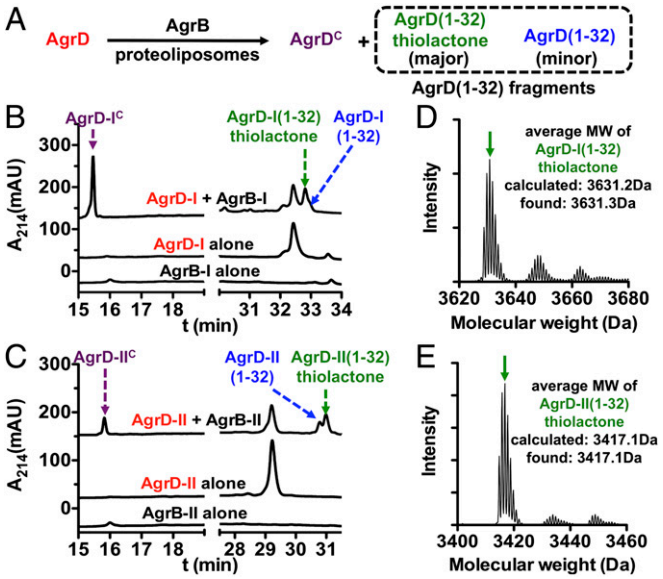

Fig. 2. AgrD(1–32)-thiolactone is the major product of AgrB-catalyzed proteolysis of AgrD. (*A*) Schematic representation of the proteolysis reaction. (*B* and *C*) C4 RP-HPLC chromatograms of the proteolysis reactions of (*B*) AgrD-I and (*C*) AgrD-II. Product peaks are indicated with arrows. (*D* and *E*) Deconvoluted MS highlighting the isotopic profile of the AgrD(1–32)-thiolactone species (green arrows) generated from (*D*) AgrD-I and (*E*) AgrD-II. MW, molecular mass.

MS as the $AgrD^C$ cleavage fragment and the thiolactone and linear AgrD(1–32) fragments. The amount of starting material and products were quantified based on integration of the RP-HPLC traces, and the molarity of each species was normalized to the starting molarity of AgrD (Fig. 3*B* and *SI Appendix*, Fig. S4*A*). During the initial stage of the reaction ($t < 10$ min), the full-length precursor AgrD was efficiently cyclized to AgrD(1–32)-thiolactone (with the concomitant release of the $AgrD^C$ fragment), whereas only small amounts of linear AgrD(1–32) were generated. The cyclization then gradually slowed down, reaching a maximum by about 30 min, which is likely caused by the dynamic equilibrium being reached (vide infra). In contrast to this equilibration behavior, the linear AgrD(1–32) was produced irreversibly at a slow but constant rate throughout the time course (Fig. 3*B*). Intriguingly, its production after $t = 30$ min was coupled to a concerted decrease in the molar fraction of AgrD and AgrD(1–32)-thiolactone (Fig. 3*B*). This kinetic observation can be understood in terms of a preequilibrium model, in which the proteolytic cyclization is a reversible process occurring much faster than the irreversible production of linear AgrD(1–32). In this model, the fast reaction reaches a quasiequilibrium state that approximates the real thermodynamic equilibrium.

To further explore the apparent reversibility of the proteolytic cyclization, we synthesized an AgrD-I^C peptide with a C-terminal carboxyamide (AgrD-I^C-NH_2) and attempted to ligate it to the recombinantly prepared AgrD-I(1–32)-thiolactone ($FlagHis_6$-tagged) (*SI Appendix*, Figs. S1*A* and S9 and Table S1) in the presence of AgrB-I proteoliposomes, thereby generating the corresponding full-length AgrD-I construct. Because this ligation product coeluted with the AgrD(1–32)-thiolactone starting material on RP-HPLC (*SI Appendix*, Fig. S4*B*), quantification of these two species relied on MS analysis using ratiometric standards (Fig. 3 *C* and *D* and *SI Appendix*, Fig. S4 *C–E*). The ligation reaction occurred rapidly, and a quasiequilibrium state was achieved within 40 min. Importantly, the postequilibration behavior of the ligation system (after $t = 40$ min) showed a marked similarity to that observed with the proteolysis reaction (compare Fig. 3*D* with Fig. 3*B*): the molar fraction of both AgrD and AgrD(1–32)-thiolactone dropped in a concerted fashion, whereas the ratio between them stayed roughly constant. This result unambiguously showed a balanced dynamic equilibrium of AgrD proteolysis under our reaction conditions.

It has been proposed that the active-site cysteine within AgrB (Cys84) attacks the scissile peptide bond in AgrD to form an acyl-enzyme intermediate that subsequently undergoes an intramolecular transthioesterification to give the AgrD(1–32)-thiolactone (Fig. 3*E*) (8). Hydrolytic resolution of this acyl-enzyme intermediate could potentially yield the linear AgrD(1–32) peptide. In accordance with this model, the inactive $AgrB^{C84A}$ mutant is unable to ligate the $AgrD^C$ peptide to AgrD(1–32)-thiolactone or hydrolyze the thiolactone (Fig. 3*C*, spectrum 1 and *SI Appendix*, Fig. S4 *F* and *G*). Therefore, we conclude that the catalytic activity of AgrB supports both the proteolysis/ligation equilibrium and the irreversible production of AgrD(1–32) (Fig. 3*E*).

We next set out to determine the equilibrium constant of the proteolytic cyclization reaction. To this end, the preequilibrium positions in the presence of different concentrations of $AgrD^C$ were monitored and plotted (Fig. 3 *F* and *G*, black circles). As expected, the preequilibrium position shifted toward the formation of full-length AgrD at higher $AgrD^C$ concentrations. Linear regression of the plot in Fig. 3*G* returned an equilibrium constant for the proteolytic cyclization ($K_{eq} = 1.0 \times 10^{-5}$) or if one treats $AgrD^C$ as a reversible ligand for the thiolactone, a dissociation constant (K_d) of 10 μM. This K_{eq} value corresponds to a $\Delta G^{0'}$ of 7.1 kcal/mol, which is 2.6 kcal/mol more favorable than expected based on our initial estimate from model reactions. Gratifyingly, the preequilibrium state obtained using AgrD as the starting material (Fig. 3*B*) conformed well to this equilibrium constant derived from the linear regression (Fig. 3*G*, red circle).

AgrD(1–32)-Thiolactone Is Stabilized by Phospholipids. Our experimentally measured equilibrium constant for proteolytic cyclization indicates that the reaction is about 70-fold more favorable than might be expected based on model reactions ($K_{eq} = 1.0 \times 10^{-5}$ vs. 1.4×10^{-7}). In an effort to gain some insight into this discrepancy, we asked whether the macrocycle within the AgrD (1–32)-thiolactone was somehow stabilized under the reaction conditions. To test this idea, we compared the susceptibility of AIP-I and $FlagHis_6$-AgrD-I(1–32)-thiolactone with ring-opening thiolysis by NAC to give the respective linear thioesters (Fig. 4*A*). Equilibration between thiolactone and linear thioester species was monitored at a series of NAC concentrations by RP-HPLC/MS. Treating NAC as a ligand that reversibly binds to the thiolactones, its dissociation constant, $K_{d,\ NAC}$, was calculated from the equilibrium positions. Importantly for the following discussion, we observed essentially unbiased partitioning of NAC between aqueous and 1-octanol phases at pH 7.5 (logP = −0.03) (*SI Appendix*, Fig. S5*A*). Thus, the effective concentration of NAC should stay constant across the bulk solution and the membrane environment.

To begin, we treated AIP-I with NAC ranging from 1.0 to 100 mM in aqueous solution buffered at pH 7.0 (Fig. 4*B*, circles and dotted line and Table 1). The $K_{d,\ NAC}$ for AIP-I is 5.8 mM. Ring closure of AIP-I from its linear thioester is, therefore, less favorable than we estimated for the formation of an unstrained thiolactone, for which the equilibrium constant would be 24 mM (Fig. 1*B*). Because AgrD-I(1–32)-thiolactone is insoluble in the buffer system used to establish the thiolysis equilibrium for AIP-I, we dispersed this molecule in a suspension of lipid vesicles in the presence of different NAC concentrations. With a calculated $K_{d,\ NAC}$ of 95 mM, this thiolactone seems to be much more stable than AIP-I (Fig. 4*B*, squares and black line and Table 1). The less favorable ring opening is not an effect of hysteresis, because reactions starting from the purified AgrD-I(1–32)-NAC thioester reached roughly the same equilibrium positions

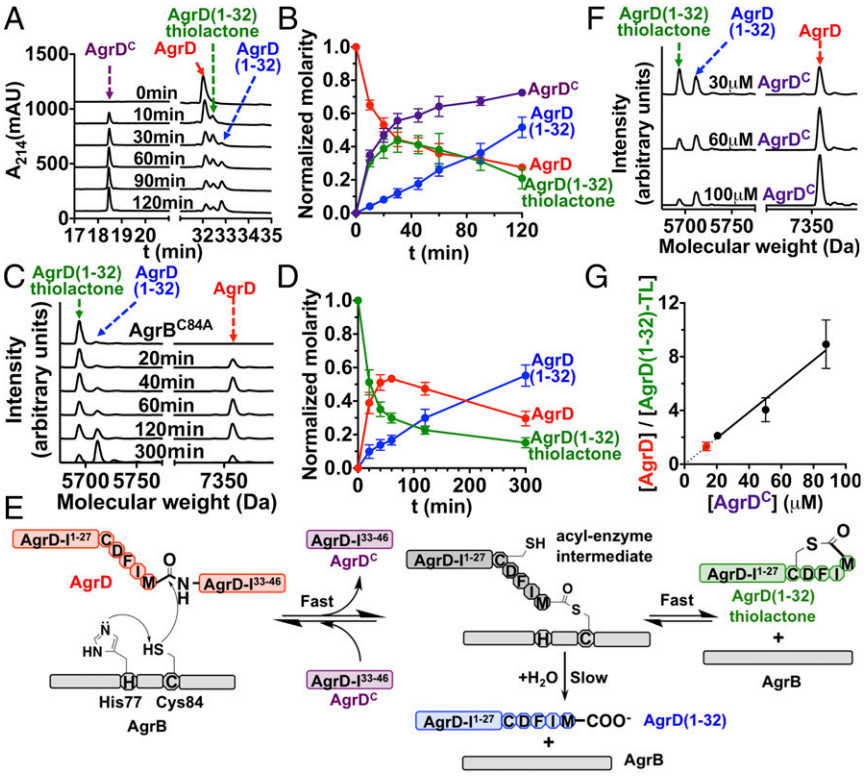

Fig. 3. AgrD processing by AgrB is a reversible process. (*A* and *B*) Time course of the proteolytic cyclization: (*A*) a representative set of RP-HPLC traces and (*B*) a kinetic plot of indicated species generated from integrated peak areas thereof are shown. In *B*, all molarity was normalized to the amount of full-length AgrD at $t = 0$. Error bars = SD ($n = 3$). (*C* and *D*) Time course of the ligation reaction: samples were resolved on RP-HPLC, and the amounts of full-length AgrD and both AgrD(1–32) fragments were quantified with MS using standards. (*C*) A representative set of deconvoluted MS spectra and (*D*) a kinetic plot of indicated species are shown. Error bars = SD ($n = 3$). (*E*) Scheme showing the mechanism of AgrB-catalyzed proteolysis of AgrD. (*F*) Ligation reactions starting at a series of $AgrD^C$ concentrations: reactions were analyzed at $t =$ 120 min, and deconvoluted mass spectra are shown as in *C*. (*G*) Plot showing the equilibrium molar ratio between AgrD and AgrD(1–32)-thiolactone as a function of the molarity of $AgrD^C$ in the ligation (black circles) and proteolysis (red circle) systems. Error bars = SD ($n = 3$).

(*SI Appendix*, Fig. S5*B*). Intriguingly, the stability of AIP-I toward ring opening was only slightly enhanced (onefold) in the presence of lipid vesicles (Fig. 4*B*, circles and black line and Table 1), despite the fact that it shares the identical macrocycle with AgrD-I(1–32)-thiolactone. It should also be noted that both thiolactones were equally susceptible to ring-opening thiolysis in aqueous buffers containing chaotropic agents (Table 1 and *SI Appendix*, Fig. S5*C*). Thus, the remarkable disparity in stability must originate from differential lipid bilayer association of the macrocycle moiety. AgrD is thought to be targeted to the lipid bilayer by its N-terminal amphipathic leader peptide (7). We confirmed this targeting effect using a comigration assay on size-exclusion chromatography (SEC), in which all AgrD constructs containing the N-terminal leader peptide showed strong interaction to bilayer nanodiscs (*SI Appendix*, Fig. S6 *A*–*C*). By contrast, AIP-I does not comigrate with nanodiscs (*SI Appendix*, Fig. S6 *D* and *E*). Based on these observations, we speculate that the membrane targeting property of the leader peptide places the macrocycle into proximity with the lipid bilayer and hence, induces its membrane partitioning, thereby stabilizing it against ring-opening thiolysis.

To explore the molecular determinants of this putative partitioning interaction, we examined atomic-resolution structures available for *S. aureus* AIPs. We noticed that, in a crystal structure determined for an mAb in complex to AIP-IV (19), three endocyclic AIP amides donate hydrogen bonds to a glutamate residue of the antibody, whereas side chains of residues Phe6, Ile7, and Met8 (all shared between AIP-IV and AIP-I) are buried in a large, contiguous hydrophobic cleft on the antibody surface (*SI Appendix*, Fig. S5 *D* and *E*). Based on this crystal structure, we envisioned that the putative partitioning of the macrocycle in the membrane might be driven by analogous interactions (specifically, the anionic phosphodiester motif in lipid head groups might form hydrogen bonds to the AIP endocyclic amide groups, and hydrophobic side chains could be embedded in the greasy interior of the bilayer) (Fig. 4*C*). In line with this model, mutating all three endocyclic hydrophobic residues to Ala

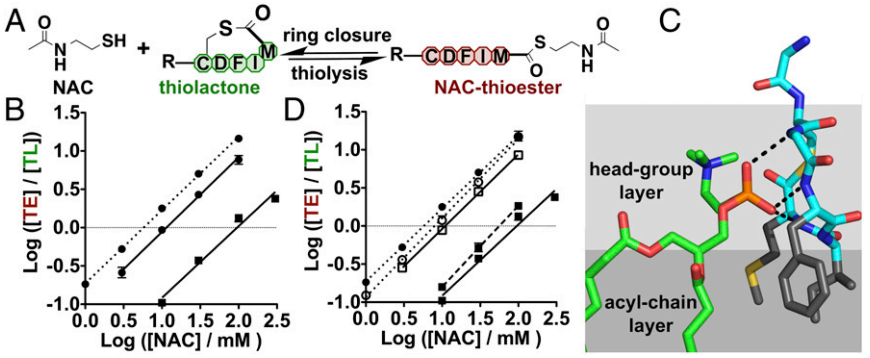

Fig. 4. Ring-opening equilibrium of AIP-I and $FlagHis_6$-AgrD-I(1–32)-thiolactone. (*A*) Schematic representation of the ring-opening equilibrium. (*B*) Double-log plot showing the thioester–thiolactone molarity ratio at the equilibrum, [TE] / [TL], as a function of NAC concentration for AIP-I (circles) or AgrD-I(1–32)-thiolactone (squares) with the absence (dotted line) or presence (black lines) of phospholipids. Error bars = SD ($n = 4$). (*C*) Stick model of AIP-I and an arbitrarily positioned POPC depicting the proposed interactions by which lipid vesicles stabilize the macrocycle: carbon atoms in POPC, AIP-I backbones, and Phe6, Ile7, and Met8 side chains are shown in green, cyan, and dark gray, respectively. Hydrogen bonds are highlighted by black dashes. Side chains of Tyr1, Ser2, Thr3, and Asp4 in AIP-I are hidden for clarity. (*D*) Like in *B*, equilibrium positions were plotted for the mutant (white symbols) or WT (black symbols) AIP-I (circles) or AgrD-I(1–32)-thiolactone (squares) in aqueous buffer alone (dotted lines) or that containing phospholipids (black lines) or glycolipids (dashed lines).

Table 1. Ring-closure equilibrium constants of thiolactones

Thiolactone and condition*	$K_{d,\ NAC}$ (mM)
AIP-I	
HBS	5.8 ± 0.2
HBS and 2 mM POPC-POPG	11.4 ± 1.1
6 M GuHCl	21.9 ± 1.4
AgrD-I(1–32)	
HBS and 2 mM POPC-POPG	95 ± 31
HBS and 2 mM digalactosidyldiacylglycerol	56 ± 7
6 M GuHCl	15.6 ± 2.2
AIP-I tri-Ala†	
HBS	8.0 ± 0.4
AgrD-I(1–32) tri-Ala†	
HBS and 2 mM POPC-POPG	11.0 ± 0.4

HBS, Hepes-buffered saline [20 mM sodium 4-(2-hydroxyethyl)-1-piperazineethanesulfonate (Hepes-Na) and 100 mM NaCl, pH 7.0].
*The POPC:POPG molar ratio is 3:1.
†Constructs bearing mutations F30A, I31A, and M32A (in AgrD-I numbering).

in AgrD-I(1–32)-thiolactone abolished stabilization of the macrocycle in the presence of liposomes (Fig. 4*D* and Table 1), although this mutant still associated with membranes, presumably through its leader sequence, which remains intact (*SI Appendix*, Fig. S6 *A–C*). Indeed, this mutant exhibited thiolysis equilibrium positions similar to those of AIP-I: either the WT peptide or that bearing the triple-Ala mutant macrocycle (Fig. 4*D* and Table 1). In addition, liposomes primarily composed of a noncharged glycolipid, digalactosidyldiacylglycerol, conferred slightly weaker stabilization to WT AgrD-I(1–32)-thiolactone than did POPC-POPG liposomes (Fig. 4*D* and Table 1). Collectively, these observations are consistent with roles for both hydrophobic and polar interactions in the stabilization of the thiolactone macrocycle as a consequence of membrane targeting.

AgrD Processing by AgrB Is a Reversible Process in Vivo, and Perturbing the Equilibrium Affects AIP Production. Finally, we asked whether the reversibility of proteolytic cyclization observed in our in vitro reconstituted system had relevance to AIP production in *S. aureus* cells. To this end, we constructed *S. aureus* plasmids for production of two AgrD-I^C peptides: one with a WT sequence and one with a scrambled sequence. These AgrD-I^C peptides were fused to a Flag-tagged ubiquitin (Ub-Flag$_2$) for detection purposes (Fig. 5*A*). Both plasmids were introduced to an *S. aureus* strain carrying an *agr-I* locus, resulting in two transformants with similar growth rates (*SI Appendix*, Fig. S7). Immunoblotting revealed the presence of AgrD-I-Ub-Flag$_2$, the expected ligation product between the AgrD-I^C construct and endogenous AgrD-I(1–32)-thiolactone, in cells expressing the WT construct (Fig. 5*B*, lanes 1–4 and red arrowhead) but importantly, not the scrambled construct (Fig. 5*B*, lanes 5–8). As expected, this ligation product was not present in transformed *agr* KO cells expressing the WT AgrD-I^C construct (Fig. 5*B*, lanes 9–12). Remarkably, AIP-I secretion was significantly lower in *agr-I* cells expressing the WT AgrD-I^C construct compared with those expressing the scrambled construct, which was determined using an *agr-I*–specific reporter gene assay (Fig. 5*C*). We interpret this as resulting from sequestration of AgrD-I(1–32)-thiolactone as a consequence of AgrB-I–mediated ligation with WT AgrD-I^C-Ub-Flag$_2$ but not the scrambled control.

Discussion

Factors That Facilitate AgrD Proteolytic Cyclization. When a polypeptide undergoes proteolysis, the peptidyl fragment N-terminal to the scissile bond is transferred to an acceptor nucleophile. Although water is, by far, the most frequent acceptor, nature also efficiently harnesses a spectrum of *N*- or *O*-nucleophiles, leading to the formation of various branched, cyclic, or C-terminally modified peptides or proteins (11). To the best of our knowledge, the first step in AIP biosynthesis is the only known proteolytic event where an *S*-nucleophile serves as the final acceptor of the peptidyl group—this definition excludes the transient, thioester-linked acyl-enzyme intermediates associated with the activity of cysteine proteases. It is noteworthy that nature typically couples ATP hydrolysis to the conversion of a carboxyl group (through an adenylation step) into a thioester (e.g., the activity of the ubiquitin activating enzyme E1) (20). In this study, we broke down the thiolactone-forming proteolysis reaction into the following half-reactions: (*i*) thiolysis of AgrD at the scissile peptide bond and (*ii*) ring closure from the resulted linear thioester (Fig. 1*B*). Using chemical equilibrium approaches, we experimentally determined the $\Delta G^{0'}$ for the overall proteolytic cyclization reaction (7.1 kcal/mol) and the ring closure from the linear AgrD(1–32)-NAC thioester (1.4 kcal/mol; calculated from $K_{d,\ NAC}$ = 95 mM). The former reaction is 2.6 kcal/mol more favorable than our estimation based on model reactions, whereas the latter is more favorable by 0.9 kcal/mol. This comparison indicates that the initial thiolysis step is also more facile (by 1.7 kcal/mol) than might be expected. To account for this difference, we propose that the scissile bond in AgrD is more sensitive to proteolysis than a generic peptide bond. Indeed, it has been shown that the free energy of hydrolysis for an individual peptide bond may vary by a few kilocalories per mole as a function of sequence context in folded proteins (21). Conceivably, targeting of AgrD to the lipid bilayer by the N-terminal leader peptide could also help sensitize the scissile amide to proteolysis caused by changes in the local chemical environment around this bond (e.g., changes in the dielectric of the medium, electrostatic effects, and so on). Additional experiments will be required to test this idea.

Physiological Implications of Our Experimental $\Delta G^{0'}$ for Thiolactone Formation. Autoinduction of the *agr* locus in *S. aureus* features an abrupt up-regulation of the effector RNA levels during the exponential growth phase (22). A recent report showed that the pheromone concentration in a liquid medium culture of a group I strain reaches 5 μM in 2 h (23). By definition, this process generates the same number of AgrD^C fragments in the cytoplasm, which leads to a considerably elevated intracellular concentration because of the much smaller volume of the cytoplasm compared with

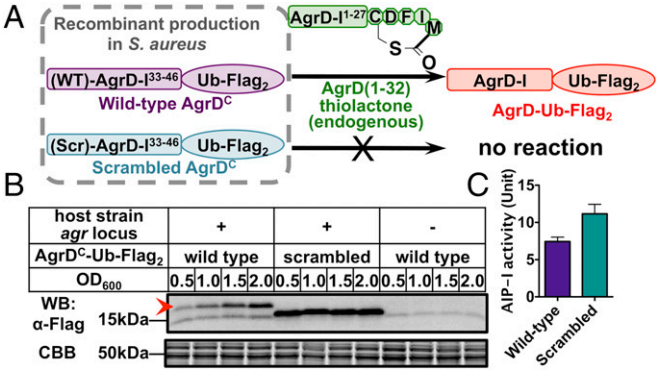

Fig. 5. Reversibility of the proteolytic cyclization in vivo. (*A*) Schematic representation of the experimental design: production in *S. aureus* of WT AgrD-I^C peptide (purple) but not the scrambled control (teal), is expected to give rise to AgrD-I-Ub-Flag$_2$ (red) through the reverse activity of AgrB-I. (*B*) Western blot (WB) analysis of cells producing AgrD-I^C peptides: *S. aureus* with indicated genotypes was grown at 30 °C to indicated OD_{600} before lysis. A high-molecular mass slice of the gel was stained with Coomassie brilliant blue (CBB) as a loading control. (*C*) Bar graph showing AIP-I activity in the medium isolated from *agr-I* cells producing indicated AgrD-I^C peptides determined by an *agr-I*–specific reporter gene assay. Error bar = SD (n = 6).

the medium. For example, $AgrD^C$ production would reach an accumulative concentration of 5 mM in 2 h at a rate of 700 nM/s assuming that 1 mL cytoplasm is present in a 1-L cell culture in late exponential phase (24). Constant and efficient AIP production, therefore, necessitates simultaneous removal of $AgrD^C$, because as we have shown, elevating the levels of this fragment can perturb the equilibrium of AgrB-mediated proteolytic cyclization (Fig. 5). Assuming that equimolar amounts of AgrD and AgrD(1–32)-thiolactone are present in a quasiequilibrium with $AgrD^C$ in postinduction *S. aureus* cells, the steady-state concentration of $AgrD^C$ should be equal to the equilibrium constant for the proteolytic cyclization, K_{eq} = 10 μM. The half-life of $AgrD^C$ would, therefore, be on the order of 10 s given a production (and degradation) rate of 700 nM/s. This short lifetime of AgrD-I^C indicates a pathway in *S. aureus* that actively targets the peptide for degradation.

The above estimation of the in vivo lifetime of $AgrD^C$ sheds light on two long-standing puzzles with respect to the production of staphylococcal AIPs. The first of these involves the observation that AIP production is greatly reduced as a consequence of genetic or chemical KO of ClpP, the catalytic subunit of certain major AAA+ proteases in *S. aureus* (25, 26). Although this phenotype has been known for more than a decade, the underlying mechanism has been elusive. We propose that ClpP constitutes the AAA+ protease that catalyzes the degradation of $AgrD^C$ and thus, fuels the proteolytic cyclization of AgrD. The second puzzle relates to the remarkable sequence conservation of $AgrD^C$ (*SI Appendix*, Fig. S8). Surprisingly, mutations at most highly conserved positions on $AgrD^C$ have no effect on the substrate recognition by AgrB (9). Given the necessity for rapid degradation of $AgrD^C$ on *agr* induction, we hypothesize that a conserved motif within $AgrD^C$ targets the peptide to the degradation machinery either through direct binding or mediated by a dedicated adaptor protein. Experimental tests of this hypothesis are currently in progress.

In conclusion, we have successfully reconstituted the first biosynthesis step en route to the production of staphylococcal AIPs. This reconstitution unambiguously confirmed that AgrB-mediated proteolysis of AgrD is directly coupled to the formation of the thiolactone macrocycle. Detailed physicochemical characterization suggests that the protease that degrades $AgrD^C$ is a critical and hitherto unappreciated participant in AIP production. Additional understanding of the biosynthetic pathway will require the identification of (*i*) the transporter that translocates the thiolactone intermediate across the cell membrane and (*ii*) the players involved in the turnover of $AgrD^C$. Methods developed in course of this study provide the starting point to address these questions.

Materials and Methods

Biochemical Assays Using AgrB Proteoliposomes. AgrB was first reconstituted to proteoliposomes as detailed in *SI Appendix*. The proteoliposomes were extensively washed and then, resuspended at 2× working concentration (2 μM AgrB) in phosphate-buffered saline [20 mM sodium phosphate, 100 mM NaCl, 2 mM tris(2-carboxyethyl)phosphine (TCEP), pH 7.5]. For ligation reactions, the suspension buffer also contained the AgrD-I^C-NH_2 peptide at 2× working concentration. To initiate a reaction, 1 volume proteoliposome suspension was mixed with 0.9 volumes phosphate-buffered saline and 0.1 volumes 400 μM stock of the appropriate substrate in DMSO. The reaction was incubated at 37 °C, and aliquots were withdrawn at indicated time points for SDS/PAGE or HPLC analysis. Details are in *SI Appendix*.

Ring-Opening Thiolysis of Thiolactone Macrocycles. At t = 0, the reaction contains 20 μM thiolactone starting material, an appropriate amount of NAC (ranging from 1 to 300 mM), 50 mM TCEP, and all of the buffer molecules indicated in Table 1. The reaction was allowed to equilibrate at 37 °C under an argon atmosphere. Aliquots were withdrawn at indicated time points for RP-HPLC analysis as detailed in *SI Appendix*.

Overproduction of AgrD-I^C-Ub-$Flag_2$ in *S. aureus*. Production of the AgrD-I^C-Ub-$Flag_2$ construct was achieved by constitutive coexpression of two proteins (Sumo-AgrD-I^C-Ub-$Flag_2$ and the yeast Sumo protease Ulp1 from a plasmid). The expression plasmids were introduced to appropriate stains using standard protocols (27). For a typical experiment, cells from an overnight culture were washed thoroughly with water, transferred to fresh media, and grown at 30 °C. Cultures removed at indicated OD_{600} were used to prepare whole-cell lysate and cell-free medium for immunoblotting or reporter gene analysis as detailed in *SI Appendix*.

ACKNOWLEDGMENTS. We thank Geeta Ram and Hope Ross for guidance on genetic experiments in *Staphylococcus aureus* and Manuel Müller, Jeffery Johnson, and Neel Shah for discussions. This work was supported by NIH Grants AI042783 and GM095880.

1. Ng WL, Bassler BL (2009) Bacterial quorum-sensing network architectures. *Annu Rev Genet* 43:197–222.
2. Novick RP, Geisinger E (2008) Quorum sensing in staphylococci. *Annu Rev Genet* 42: 541–564.
3. Thoendel M, Kavanaugh JS, Flack CE, Horswill AR (2011) Peptide signaling in the staphylococci. *Chem Rev* 111(1):117–151.
4. Ji G, et al. (2005) Staphylococcus intermedius produces a functional agr autoinducing peptide containing a cyclic lactone. *J Bacteriol* 187(9):3139–3150.
5. Wuster A, Babu MM (2008) Conservation and evolutionary dynamics of the agr cell-to-cell communication system across firmicutes. *J Bacteriol* 190(2):743–746.
6. Ji G, Beavis R, Novick RP (1997) Bacterial interference caused by autoinducing peptide variants. *Science* 276(5321):2027–2030.
7. Zhang L, Lin J, Ji G (2004) Membrane anchoring of the AgrD N-terminal amphipathic region is required for its processing to produce a quorum-sensing pheromone in Staphylococcus aureus. *J Biol Chem* 279(19):19448–19456.
8. Qiu R, Pei W, Zhang L, Lin J, Ji G (2005) Identification of the putative staphylococcal AgrB catalytic residues involving the proteolytic cleavage of AgrD to generate autoinducing peptide. *J Biol Chem* 280(17):16695–16704.
9. Thoendel M, Horswill AR (2009) Identification of Staphylococcus aureus AgrD residues required for autoinducing peptide biosynthesis. *J Biol Chem* 284(33):21828–21838.
10. Kavanaugh JS, Thoendel M, Horswill AR (2007) A role for type I signal peptidase in Staphylococcus aureus quorum sensing. *Mol Microbiol* 65(3):780–798.
11. Arnison PG, et al. (2013) Ribosomally synthesized and post-translationally modified peptide natural products: Overview and recommendations for a universal nomenclature. *Nat Prod Rep* 30(1):108–160.
12. Thoendel M, Horswill AR (2013) Random mutagenesis and topology analysis of the autoinducing peptide biosynthesis proteins in Staphylococcus aureus. *Mol Microbiol* 87(2):318–337.
13. Lehninger AL, Nelson DL (2008) Lehninger's Principles of Biochemistry (Freeman, New York), 5th Ed.
14. Martin RB (1998) Free energies and equilibria of peptide bond hydrolysis and formation. *Biopolymers* 45(5):351–353.
15. Illuminati G, Mandolini L (1981) Ring-closure reactions of bifunctional chain molecules. *Acc Chem Res* 14(4):95–102.
16. Jarraud S, et al. (2000) Exfoliatin-producing strains define a fourth agr specificity group in Staphylococcus aureus. *J Bacteriol* 182(22):6517–6522.
17. Boldog T, Grimme S, Li M, Sligar SG, Hazelbauer GL (2006) Nanodiscs separate chemoreceptor oligomeric states and reveal their signaling properties. *Proc Natl Acad Sci USA* 103(31):11509–11514.
18. Wang B, Zhao A, Novick RP, Muir TW (2014) Activation and inhibition of the receptor histidine kinase AgrC occurs through opposite helical transduction motions. *Mol Cell* 53(6):929–940.
19. Kirchdoerfer RN, et al. (2011) Structural basis for ligand recognition and discrimination of a quorum-quenching antibody. *J Biol Chem* 286(19):17351–17358.
20. Scheffner M, Nuber U, Huibregtse JM (1995) Protein ubiquitination involving an E1-E2-E3 enzyme ubiquitin thioester cascade. *Nature* 373(6509):81–83.
21. Buczek O, Krowarsch D, Otlewski J (2002) Thermodynamics of single peptide bond cleavage in bovine pancreatic trypsin inhibitor (BPTI). *Protein Sci* 11(4):924–932.
22. Ziebandt AK, et al. (2004) The influence of agr and sigmaB in growth phase dependent regulation of virulence factors in Staphylococcus aureus. *Proteomics* 4(10):3034–3047.
23. Junio HA, et al. (2013) Quantitative analysis of autoinducing peptide I (AIP-I) from Staphylococcus aureus cultures using ultrahigh performance liquid chromatography-high resolving power mass spectrometry. *J Chromatogr B Analyt Technol Biomed Life Sci* 930:7–12.
24. Maass S, et al. (2011) Efficient, global-scale quantification of absolute protein amounts by integration of targeted mass spectrometry and two-dimensional gel-based proteomics. *Anal Chem* 83(7):2677–2684.
25. Frees D, Qazi SNA, Hill PJ, Ingmer H (2003) Alternative roles of ClpX and ClpP in Staphylococcus aureus stress tolerance and virulence. *Mol Microbiol* 48(6):1565–1578.
26. Böttcher T, Sieber SA (2008) Beta-lactones as specific inhibitors of ClpP attenuate the production of extracellular virulence factors of Staphylococcus aureus. *J Am Chem Soc* 130(44):14400–14401.
27. Ram G, et al. (2012) Staphylococcal pathogenicity island interference with helper phage reproduction is a paradigm of molecular parasitism. *Proc Natl Acad Sci USA* 109(40):16300–16305.